XMM−Newton Observations of the Galactic Supernova Remnant CTB 109

M. Sasaki, P.P. Plucinsky, T.J. Gaetz, R.K. Smith, R.J. Edgar, P.O. Slane

Harvard−Smithsonian Center for Astrophysics

The Galactic supernova remnant (SNR) CTB 109 is thought to be interacting with a molecular cloud complex. As no X−ray emission is observed from the western part of the remnant shell, the outer blast wave has apparently been stopped by the cloud complex on this side. Inside the shell, CTB 109 has an X−ray bright region in the east, known as the 'Lobe' or the 'Jet'. We present the results from the XMM AO1 observations of SNR CTB 109. The XMM EPIC spectra of the 'Lobe' shows that its emission is thermal and the spectral variations are probably caused by differences in temperature or in the ionization timescale of plasma. The spectra clearly show Mg and Si lines in the whole Lobe region. The enhanced X−ray emission of the 'Lobe' is indicative of an interaction of the SNR shock wave with a molecular cloud. Furthermore, we derived values for e.g. shock velocity or column density from EPIC spectra of the SNR shell. The interaction of the shock with the surrounding medium is discussed. This work was supported by CXC contract NAS8−39703 and Chandra grant GO0−1127X.

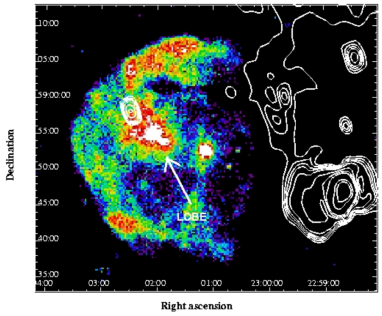

Figure 1: ROSAT PSPC images of CTB 109 with contours of IRAS data.

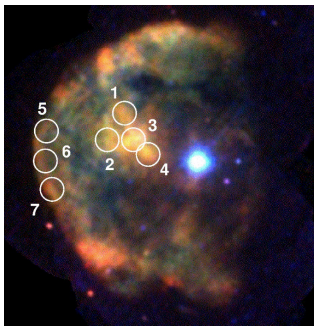

Figure 2: XMM EPIC true color image (red: 0.3 −0.9 keV, green: 0.9 − 1.5 keV, blue: 1.5 − 4.0 keV) with extracted regions.

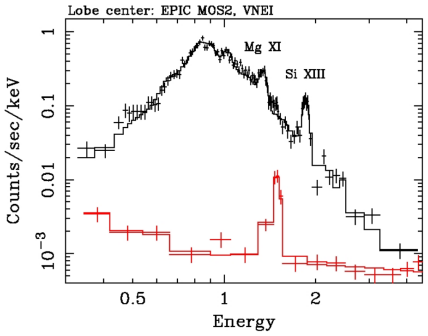

Figure 3: EPIC MOS2 spectrum of region 3, extracted from the data of observation 0155350301 (black: source+background, red: background).

Introduction

- SNR CTB 109 (G109.1−1.0) has a semi−circular morphology in both the X−rays and the radio and is the host remnant of the anomalous X−ray pulsar 1E2259+586.
- It is associated with a giant molecular cloud (GMC) complex (Heydari−Malayeri et al., 1981).
- Radio shell does not extend further to the west behind the GMC (Gregory et al., 1983; Hughes et al., 1984). ⇒ The SNR shock has been stopped by the GMC complex on one side.
- CO observations by Tatematsu et al. (1990) showed that there is an extension of the GMC (CO 'arm'), coincident with the local X−ray minimum in the north of the pulsar. ⇒ This part of the cloud lies in front of the remnant.
- Bright, interior region in X−rays: the 'Lobe'.
  - A jet from the pulsar? (Gregory & Fahlman, 1980)
  - ROSAT HRI and Chandra images (Hurford & Fesen, 1995; Patel et al., 2001): no morphological connection between the Lobe and the pulsar.
  - BBXRT and ROSAT spectra of the Lobe showed that the emission is thermal in origin, arguing against a jet interpretation (Rho & Petre, 1997).
- An enhancement coincident with the Lobe was detected in the IRAS data (Coe et al., 1989): Figure 1 shows an overlay of IRAS contours on a ROSAT image. The IR bright spot is located at the northeastern end of the Lobe region.
- The bright X−ray emission from the Lobe is most likely caused by a density enhancement in material which was shocked by the blast wave.

XMM−Newton data

- EPIC data of three AO 1 Pointings: south, north, and east, with exposure times of ~11, 10, 10 ks, respectively.
- Additional pointing (0155350301) towards the pulsar in the XMM Archive with 18 ks of MOS2 data.
- True color image (Figure 2):
  - CTB 109 has no emission in the west.
  - In the interior, the Lobe is very bright.
  - Dark regions north and south of the Lobe.
  - Around the outskirts of the Lobe the data appear redder on the western side, indicating a softer X−ray spectrum.
  - On the eastern side, the outskirts appear a little greener, indicating a harder spectrum.

EPIC spectrum of the Lobe

- There are differences in temperature, ionization timescale nt of the plasma, and/or absorbing column density N_H in different parts of the Lobe (Table 1).
- The XMM spectra of the Lobe fit better with a single−temperature non−equilibrium ionization model (VNEI) than with a collisional ionization equilibrium model (VMEKAL).
- In the northern part (reg. 1), N_H is marginally higher and nt lower than in the rest of the Lobe.
- In the bright central part (reg. 3, see also Fig. 3), Si appears to be overabundant (1.7±0.4 times solar), while the Mg abundance is consistent with solar.
- This is not what we would expect if the byproducts of dust destruction were contributing to the X−ray emitting material, because we expect Mg and Si to be similar.
- The abundances are mostly consistent with solar which is not what we expect for ejecta.

Spectral analysis of the eastern shell

- The eastern shell has the largest distance to the pulsar and is located opposite to the GMC complex in the west. ⇒It corresponds to the blast wave propagating into a lower density ISM (Kothes et al., 2002).
- In regions 5 − 7, kT obtained for the thermal emission model is ~0.60 − 0.65 keV, thus higher than in the Lobe.
- The Mg and Si abundances are almost consistent with solar values, and nt is ~1×10^{11}s cm^{-3}, i.e. lower than in the Lobe.

Calculations based on Sedov solution

- Assume self−similarity and jump condition at the shock front.
- Distance to CTB 109: D = 3 kpc (Kothes et al., 2002).
- Radius of the eastern shell, from image: R_S = 1112" = 16.2 pc.
- Temperature, from EPIC (PN and MOS1/2) spectra of regions 5 and 6 : T = 0.65 keV = 7.54×10^6 K.
- Shock velocity: $T = (3\mu)/(16R)\ v_S^2 \Rightarrow v_S$ = 485 km/s.
- Age: $v_S = dR_S/dt = (2R_S)/(5t)$ $\Rightarrow t = 4.12\times10^{11}$ s = 1.31×10^4 yrs.

Table 1: XMM spectral results of the **Lobe** from MOS2 data of the observation 0155350301. Used spectral models are **VMEKAL** and **VNEI**, both with solar abundances except for Mg and Si.

Region	$N_H(10^{22})$ [cm^{-2}]	kT [keV]	Mg (solar)	Si (solar)	$nt(10^{11})$ [s cm^{-3}]	χ^2/d.o.f
MOS2 (0155350301), **VMEKAL**						
1 (North)	$0.42^{+0.06}_{-0.07}$	$0.60^{+0.03}_{-0.03}$	$1.9^{+0.5}_{-0.5}$	$1.0^{+0.5}_{-0.6}$	–	186.5/98 = 1.9
2 (East)	$0.40^{+0.04}_{-0.04}$	$0.60^{+0.02}_{-0.02}$	$1.8^{+0.4}_{-0.4}$	$1.0^{+0.3}_{-0.3}$	–	150.5/95 = 1.6
3 (Center)	$0.38^{+0.08}_{-0.08}$	$0.54^{+0.06}_{-0.02}$	$1.7^{+0.3}_{-0.2}$	$1.6^{+0.3}_{-0.4}$	–	246.8/116 = 2.1
4 (Southwest)	$0.40^{+0.04}_{-0.03}$	$0.51^{+0.03}_{-0.02}$	$1.5^{+0.3}_{-0.2}$	$1.4^{+0.3}_{-0.4}$	–	169.1/108 = 1.6
MOS2 (0155350301), **VNEI**						
1 (North)	$0.61^{+0.10}_{-0.08}$	$0.58^{+0.05}_{-0.03}$	$0.9^{+0.3}_{-0.2}$	$1.0^{+0.3}_{-0.3}$	$1.3^{+0.5}_{-0.4}$	154.5/97 = 1.6
2 (East)	$0.47^{+0.07}_{-0.06}$	$0.59^{+0.04}_{-0.03}$	$1.1^{+0.3}_{-0.2}$	$1.1^{+0.4}_{-0.3}$	$2.5^{+2.8}_{-0.9}$	100.0/94 = 1.1
3 (Center)	$0.48^{+0.09}_{-0.05}$	$0.56^{+0.03}_{-0.03}$	$1.0^{+0.3}_{-0.1}$	$1.7^{+0.3}_{-0.4}$	$1.9^{+0.5}_{-0.5}$	152.1/115 = 1.3
4 (Southwest)	$0.46^{+0.08}_{-0.05}$	$0.52^{+0.03}_{-0.06}$	$1.0^{+0.2}_{-0.2}$	$1.5^{+0.4}_{-0.4}$	$2.9^{+1.3}_{-0.7}$	113.1/107 = 1.1

Table 2: XMM spectral results of circular regions of the eastern shell, extracted from the east pointing data. Used spectral models are **VMEKAL** and **VNEI** with solar abundances except for Mg and Si.

Region	$N_H(10^{22})$ [cm^{-2}]	kT [keV]	Mg (solar)	Si (solar)	$nt(10^{11})$ [s cm^{-3}]	χ^2/d.o.f
EPIC all (east), **VMEKAL**						
5	$0.47^{+0.01}_{-0.09}$	$0.60^{+0.02}_{-0.01}$	$1.9^{+0.3}_{-0.2}$	$1.0^{+0.2}_{-0.2}$	–	1209.4/880 = 1.4
6	$0.47^{+0.01}_{-0.13}$	$0.59^{+0.01}_{-0.02}$	$1.7^{+0.1}_{-0.4}$	$0.9^{+0.2}_{-0.3}$	–	1468.5/1082 = 1.4
7	$0.30^{+0.05}_{-0.05}$	$0.60^{+0.02}_{-0.02}$	$2.2^{+0.3}_{-0.3}$	$1.1^{+0.4}_{-0.2}$	–	1513.4/952 = 1.6
EPIC all (east), **VNEI**						
5	$0.65^{+0.10}_{-0.10}$	$0.65^{+0.08}_{-0.08}$	$1.0^{+0.1}_{-0.2}$	$0.8^{+0.2}_{-0.2}$	$1.0^{+0.5}_{-0.7}$	1155.4/879 = 1.3
6	$0.62^{+0.25}_{-0.22}$	$0.65^{+0.22}_{-0.41}$	$1.0^{+0.1}_{-0.3}$	$1.0^{+0.1}_{-0.3}$	$0.9^{+1.7}_{-0.6}$	1381.2/1081 = 1.3
7	$0.52^{+0.05}_{-0.08}$	$0.58^{+0.06}_{-0.02}$	$1.0^{+0.3}_{-0.2}$	$0.9^{+0.3}_{-0.3}$	$1.2^{+0.2}_{-0.1}$	1363.0/951 = 1.4
PN (east), **VNEI**						
5	$0.60^{+0.10}_{-0.08}$	$0.65^{+0.12}_{-0.07}$	$1.0^{+0.2}_{-0.2}$	$0.9^{+0.2}_{-0.3}$	$1.0^{+0.1}_{-0.1}$	413.3/321 = 1.3
6	$0.58^{+0.08}_{-0.08}$	$0.61^{+0.02}_{-0.02}$	$0.8^{+0.1}_{-0.1}$	$0.8^{+0.2}_{-0.2}$	$1.3^{+0.2}_{-0.2}$	653.0/482 = 1.4
7	$0.48^{+0.06}_{-0.06}$	$0.61^{+0.05}_{-0.05}$	$1.2^{+0.2}_{-0.2}$	$0.9^{+0.2}_{-0.3}$	$1.1^{+0.2}_{-0.2}$	491.9/340 = 1.4
MOS1/2 (east), **VNEI**						
5	$0.68^{+0.09}_{-0.04}$	$0.66^{+0.07}_{-0.07}$	$1.0^{+0.1}_{-0.2}$	$0.8^{+0.3}_{-0.2}$	$0.8^{+0.2}_{-0.3}$	733.9/552 = 1.3
6	$0.67^{+0.37}_{-0.15}$	$0.62^{+0.16}_{-0.39}$	$1.1^{+0.5}_{-0.2}$	$1.0^{+0.4}_{-0.9}$	$0.7^{+1.1}_{-0.4}$	946.1/593 = 1.6
7	$0.52^{+0.58}_{-0.14}$	$0.58^{+0.19}_{-0.39}$	$1.0^{+0.3}_{-0.5}$	$1.0^{+0.8}_{-0.7}$	$1.3^{+1.5}_{-0.9}$	898.2/340 = 1.5

References

- Coe, M.J. et al. 1989, MNRAS, 238, 649
- Gregory, P.C., & Fahlman, G.C. 1980, Nature, 287, 805
- Gregory, P.C. et al. 1983, in *'Supernova Remnants and their X−ray Emission'*, eds. I.J. Danzinger & P. Gorenstein (Dordrecht: Reidel), 437
- Heydari−Malayeri, M. et al. 1981, Nature 293, 549
- Hughes, V.A. et al. 1984, ApJ, 283, 147
- Hurford, A.P. & Fesen, R.A. 1995, MNRAS, 277, 549
- Kothes, R. et al. 2002, ApJ, 576, 169
- Patel, S.K. et al. 2001, ApJ, 563, L45
- Rho, J. & Petre, R. 1997, ApJ, 484, 828
- Tatematsu, K. et al. 1990, ApJ, 351, 157